Article

Green Synthesis and Characterization of ZnO Nanoparticles by Using Thyme Plant Leaf Extract

Shayma Tahsin Karam and Ahmed Fattah Abdulrahman * ![ORCID]

Department of Physics, Faculty of Science, University of Zakho, Zakho 42002, Iraq
* Correspondence: ahmed.abdulrahman@uoz.edu.krd

Abstract: Zinc oxide (ZnO) nanoparticles (NPs) were fabricated by using leaves extracted from the thyme plant by employing a green method. The influence of several calcination (annealing) temperatures on the characteristic properties of fabricated ZnO NPs and the optimum calcination temperature for growing ZnO NPs were studied and reported. The studied calcination temperatures were 150 °C, 250 °C, 350 °C, and 450 °C. Different characterization techniques were used to study and examine the properties of biosynthesized ZnO NPs by using thyme plant leaf extract. The results of each UV-Vis analysis and FTIR spectrum of the leaf extract of the thyme plant confirmed and suggested that the selected leaf extract of thyme is a practicable choice for green synthesis of ZnO NPs. The investigated UV-Vis spectra of plant leaf extract displayed two strong absorption peaks at 266 nm and 313 nm at ambient temperature. The results of FESEM images showed that the calcination temperature has a significant and large effect on the morphology, size, shape, and orientation of ZnO NPs, which have a spherical shape with an average size in the range of 39.4–51.86 nm. In addition, the XRD results confirm that the ZnO NPs formed are pure ZnO with wurtzite hexagonal structure with particle size along the (002) peak in the range of 35.20–243.3 nm. The results of UV-Vis of ZnO NPs displayed a strong peak for all ZnO NPs produced at different calcination temperatures, a high absorbance in the UV region below 400 nm, and a low absorbance rate in the visible range. The obtained energy band gap (Eg) was in the range of 2.645–2.7 eV. In addition, the results of the FTIR spectra of ZnO NPs at different calcination temperatures revealed there was no discernible peak in the monitoring range, which indicated the purity of the ZnO nanoparticles generated via using thyme leaf extract. In addition, from all obtained results of the fabricated ZnO NPs, the ZnO NPs synthesized at the calcination temperature of 450 °C showed a high quality and improvement compared to the ZnO NPs synthesized at other calcination temperatures.

Keywords: green method; calcination temperature; thyme; extraction; ZnO NPs

1. Introduction

Nanotechnology has lately had a significant impact on several sectors, and utilizing nanomaterial development aimed at multifunctional applications in a range of disciplines is a major concern. Nanomaterials (NMs) are composed of nanoscale particles and have dimensions of 1 to 100 nm, while nanoparticles (NPs) are very tiny particles with improved catalytic reactivity, chemical stability, thermal conductivity, and nonlinear optical performance owing to their enormous surface area to unit volume ratio [1]. Nanoparticles are sometimes known to be used as nano-antibiotics due to their antibacterial capabilities [2]. Nanoparticles have found their way into a variety of industries, including chemical, food, health, feed, space, and cosmetics, necessitating a green and environmentally friendly approach to their production [3]. Nanoparticles can be synthesized from different metals in addition to metal oxides such as Pt, Cu, Ag, Pd, NiO, CuO, Au, TiO2, and ZnO [4]. Among these metal oxide and metal NPs, zinc oxide (ZnO) NPs have attracted great attention over the last two to three years owing to their low-cost production, ease of preparation, and safety, along with their wide variability of applications in biomedical systems, electronics, and optics [5–8]. ZnO is a

semiconductor utilizing a hexagonal unit cell and wurtzite structure that crystallizes. ZnO has unique features, together with a wide and straight band gap (3.36 eV), At normal temperature, it has high exciton binding energy (60 meV), a large electrochemical coupling coefficient, low toxicity, biocompatibility, and great photostability [9]. Because of these qualities, ZnO has been employed in several ground-breaking optical and electrical devices [10–13]. The quantum confinement effect gives ZnO even more fascinating features as its size approaches the nanoscale. ZnO nanoparticles have been revealed in several studies to exhibit strong antibacterial activity against a range of dangerous bacteria, making them a potential choice for several medical applications [14–17]. ZnO NPs are also commonly used in popular photocatalytic applications as a result of their strong photodegradation activity aimed at a range of organic dyes [18,19].

ZnO NPs may be made using a variety of chemical, physical, and biological methods. These technologies or methods include physical vapor deposition, hydrothermal processes, microemulsion, precipitation, chemical reduction, ultrasonic irradiation, plasma, and sol–gel. These methods commonly necessitate high temperature, high pressure, hazardous chemicals, and a considerable amount of energy, all of which are associated with negative environmental significance. Consequently, due to the need for additional robust equipment, product costs are greater [20–22]. As a result of the rising interest in environmental protection, there is a demand for environmentally friendly synthesis procedures that do not utilize toxic components. Green synthesis, a biosynthetic process, has aroused the interest of many scholars recently. When compared to traditional physical/chemical techniques, this method has several benefits, such as the diagnosis and treatment of several diseases, over and above serving as building blocks for future generations of treatments, owing to its low cost, large-scale production potential, environmentally friendly nature, simplicity, lack of additional chemicals, and the production of more stable and biocompatible nanoparticles [23–25]. Furthermore, leveraging natural resources to address environmental concerns is one of the key goals of employing green sources to manufacture nanomaterials. For example, green magnetite NPs are used to remove arsenic from water and to break down harmful chlorinated organic solvents, and the particles may be easily removed using a magnet. Nanomaterials can be used to make sensors for contaminants such as coliform bacteria or lead, making analysis easier and lowering detection limits compared to conventional analytical methods [26]. Among the several biosynthetic processes (enzymes, fungi, bacteria, etc.) known to date, green synthesis employing natural strains besides plant extracts is the greatest promising green method [20]. Zinc oxide NPs have been made from a variety of plant components, including the seed, fruit, leaf, stem, and root, because of the distinct phytochemicals they produce. Natural harvesting of all parts of the plant is a very easy, low-cost method that is extremely eco-friendly and does not involve the use of any intermediary base groups. It takes a fraction of the time; requires no costly equipment or precursors; and produces a highly pure, quantity-enriched, and contaminant-free product [27].

Phytochemicals are abundant in each portion of the plant's extract, which operates as both a stabilizing and reducing agent [28]. Plants are the most favored source of NP synthesis since they allow large-scale production along with the generation of stable NPs of a variety of sizes and shapes [29]. Metal ions or metal oxides are reduced to zero-valence metal NPs using phytochemicals such as terpenoids, vitamins, amino acids, alkaloids, polyphenolic compounds, and polysaccharides generated by plants [27,29,30]. A slew of research on the biosynthesis of ZnO NPs utilizing various kinds of natural plant extracts has newly been published; in addition, the findings establish that the features of the biosynthesized samples vary depending on the source plant extract [31]. In the current study, the leaf extract of the thyme plant has been used to biosynthesize ZnO nanoparticles in the Barwari Bala region, Terwanish Village, Duhok Government, Kurdistan Region, Iraq. Thyme is the dried aerial parts of numerous scented perennial evergreen plants in the Lamiaceae family of mints belonging to the *Thymus* genus. *Thymus* and the *Origanum* genus are indigenous to the Mediterranean. *Thymus vulgaris* is the most frequently cultivated and used herb in the culinary world, as well as being used for medicinal and

ornamental applications [32]. Using a green synthesis process, ZnO nanoparticles of various morphologies, shapes, sizes, and orientations may be produced. Different parameters such as pH value, precursor concentration, doping, quenching impact, reaction duration, reaction temperature, calcination (annealing) temperature, and reaction temperature may be optimized to regulate and improve these morphological features [33]. Additionally, inherent defects in ZnO semiconductors consist of zinc and oxygen vacancies, in addition to zinc and oxygen interstitials [34]. Calcination (annealing) temperatures are considered to be capable of eliminating and correcting these faults or impurities, activating the dopant atom, and enhancing the electrical and optical properties of ZnO NPs, which may be changed depending on the applications [35,36]. In the current research, the ZnO nanoparticles were fabricated by utilizing a green technique by employing leaf extract of the thyme plant. In addition, the impact of the four different calcination temperatures (150 °C to 450 °C) on the properties of ZnO NPs produced by the green procedure was investigated. The effect of the difference in calcination temperature on ZnO NP quality was investigated and the optimum calcination temperature for the green synthesis of ZnO NPs was determined. The relevance of this study is that the green synthesis of ZnO nanoparticles from thyme plant leaf extract might be used for photocatalysis, water pollution removal, medicinal (antibacterial) applications, solar cells, and cosmetic applications.

2. Experimental Details

Sigma-Aldrich provided zinc nitrate hexahydrate salt [Zn (NO3)2.6H2O] with a molecular weight (MW) of 297.48 g/mol and sodium hydroxide (NaOH) with a molecular weight (MW) of 40.00 g/mol, which were used without additional purification. An MR Hei-End heater–magnetic stirrer (MR Hei-End heater–magnetic stirrer (Deutschland, Germany), an EBA-20 Hettich centrifuge (Darmstadt, Germany), an S15H ultrasonic bath (Holzwickede, Germany), and a Memmert-00-800 laboratory oven (Frankenplatz, Germany) were utilized for the preparation and green synthesis of ZnO nanoparticles.

2.1. Preparation of Thyme Leaf Extract

The ZnO nanoparticles were biosynthesized utilizing the thyme plant, which was gathered in the Barwari Bala area, Terwanish Village, Duhok Government, Kurdistan Region, Iraq. Thyme is the dried aerial parts of numerous species of scented perennial evergreen herbs in the Lamiaceae family of mints belonging to the genus *Thymus*. The leaves of the thyme plant were washed several times to remove all pollution and dust before being dried and ground into powder. Additionally, 50 g of thyme plant leaf powder was added to 500 mL of double-distilled water and boiled at 75 °C for 30 min using a magnetic stirrer and heater to achieve the right extract of thyme plant leaves. The leaf extract was filtered and centrifuged extensively [37,38]. The process of harvesting thyme plant leaves is presented in Figure 1.

2.2. Green Synthesis of ZnO Nanoparticles

The ZnO NPs were produced by employing a green technique (synthesis) and thyme plant leaves extracted at various calcination temperatures (annealing). After the steps outlined in the previous section for acquiring the extract of thyme plant leaves, 50 mL thyme leaf extract was added dropwise to the 0.1 M [Zn (NO3)26H2O] solution 1:1 at room temperature for 1 h with a magnetic stirrer. Afterward, the leaf extract was well mixed with zinc salt solution to become a homogeneous solution, and the pH of the mixture was regulated and adjusted to pH 8 using sodium hydroxide (NaOH) under magnetic stirring. The color of the combination turned milky white, and then the mixture (solution) was heated at 80 °C for 3 h to obtain a brownish paste. The nucleation and reactivity of the ZnO nanoparticles occur when they form a brownish paste [37,38]. Consequently, the solution's white color grew brighter, indicating the fabricated ZnO NPs have different sizes and shapes. The sedimentation of the growth fluid separated from the ZnO NPs via centrifugation at 10,000 rpm. The powder solid was removed by employing methanol.

On top of ethanol, distilled water can be used numerous times to remove any remaining pollutants or organic materials [37]. Lastly, the ZnO powder was calcined (annealed) for 2 h at various temperatures of 150 °C, 250 °C, 350 °C, and 450 °C. The samples were labeled using the letters a, b, c, and d. Before being kept at 100 degrees Celsius, the ZnO nanoparticle powder was washed numerous times with ethanol and double-distilled water [37,38]. The ZnO NPs were produced and were ready to be examined and characterized. The green manufacturing of ZnO nanoparticles using thyme plant leaf extract is depicted in Figure 1.

Figure 1. Schematic representation of green synthesis process of ZnO NPs by using the leaf extract of thyme plant and zinc nitrate hexahydrate.

2.3. Characterization of ZnO Nanoparticles

The optical characteristics of the plant leaf extract and ZnO NPs were investigated using an Agilent Technologies Carrier Series UV-Visible double-beam spectrophotometer (Cary 100 UV-Vis). It was used for investigating the optical characteristics of ZnO and also measures wavelengths between 200 and 800 nanometers. The distinct functional groups existing in the thyme extract of plant leaves in addition to ZnO NPs synthesized at numerous calcination (annealing) temperatures were gained and observed using Fourier transform infrared spectroscopy (FTIR) (Nicolet IS 10, Thermo Scientific, Waltham, MA, USA) in the 400–4000 cm^{-1} range. The size, surface, chemical composition, shape, and orientation of ZnO nanoparticles were observed and considered using energy-dispersive X-ray spectroscopy (EDX) and field emission scanning electron microscopy (FE-SEM) (Carl Zeiss AG (Supra 55VP) using an acceleration voltage of 5–30 kV). The high-resolution X-ray diffraction (HR-XRD) system model Pro MRD, PAN X-Pert, was used to investigate the size and crystal structure, epitaxial growth goodness (quality), strain, and stress of produced ZnO NPs at varied calcination (annealing) temperatures. CuK radiation has a wavelength of 1.54050 angstrom, a scanning angle of 20–80°, and a wavelength of 2θ.

The Debye–Scherrer equation was used to determine the average particle size of ZnO NPs for the significant diffraction peaks (100), (002), and (101) [39], and the investigated results are listed in Table 1.

$$D = \frac{k\lambda}{\beta \cos \theta} \tag{1}$$

where, in turn, K and D stand for the full width at half maximum (FWHM) of the peak, diffraction angle, X-ray beam wavelength, and crystallite size shape factor.

Table 1. The particle size, volume, dislocation density, and bond length at stronger diffraction peaks for the (100), (002), and (101) planes of the ZnO nanoparticles synthesized at different calcination temperatures.

Sample	Peaks	D (nm)	V(Å3)	$\delta \times 10^{-6}$ (Å-2)	L (Å)
150 °C	100	69.913	52.149	2.046	2.0414
250 °C	100	23.309	52.310	1.841	2.0435
350 °C	100	59.919	52.146	2.785	2.0413
450 °C	100	43.021	51.422	5.403	2.0318
150 °C	002	35.202	41.041	8.069	1.8847
250 °C	002	35.203	40.993	8.069	1.8839
350 °C	002	42.249	41.038	5.602	1.8846
450 °C	002	43.308	40.988	5.332	1.8839
150 °C	101	47.189	35.272	4.490	1.7919
250 °C	101	35.384	35.208	7.990	1.7911
350 °C	101	35.381	35.291	7.990	1.7921
450 °C	101	29.021	35.185	1.190	1.7904

The number of defects caused by internal strain and substrate–crystal growth mismatch is represented by the dislocation density (δ), which can be calculated using the following equation, together with the dislocation density of produced ZnO NPs [39]:

$$\delta = \frac{1}{D^2} \tag{2}$$

where D is crystallite size. The obtained results are listed in Table 1.

The effects of the different calcination temperatures on the bond length and hexagonal-cell volume along the major and dominant diffraction peaks (100), (002), and (101) of the produced ZnO NPs were calculated from the following equations [40], and the results obtained for both are shown in Table 1.

$$L = \sqrt{\frac{a^2}{3} + \left(\frac{1}{2} - u\right)^2 c^2} \tag{3}$$

By utilizing the formula below, it is assumed that the lengthways "c" axis is also a parameter connected to the c/a ratio where u is a parameter quantifying how far one atom has traveled in the direction of the next [40];

$$u = \frac{a^2}{3c^2} + 0.25 \tag{4}$$

The following formula was used to explore the volume (V) of a hexagonal cell [40]:

$$V = \frac{\sqrt{3}}{2} a^2 c \tag{5}$$

The lattice constants (a and c) along the major and dominant diffraction peaks (100), (002), and (101) of the hexagonal ZnO NP structure were investigated using Bragg's law [40], and the results obtained are listed in Table 2.

$$a = \sqrt{\frac{1}{3}} \frac{\lambda}{\sin \theta} \tag{6}$$

$$c = \frac{\lambda}{\sin \theta} \tag{7}$$

Table 2. Lattice parameters of ZnO wurtzite–hexagonal structure characteristics at stronger diffraction peaks for the (100), (002), and (101) planes of the ZnO nanoparticles synthesized at different calcination temperatures.

Sample	Peaks	FWHM	2θ	c (Å)	ε_c%	a (Å)	ε_a%	d (Å)
150 °C	100	0.1181	31.6293	5.653	8.628	3.264	0.455	2.827
250 °C	100	0.3542	31.5961	5.659	8.739	3.267	0.558	2.829
350 °C	100	0.1378	31.6301	5.653	8.626	3.264	0.452	2.826
450 °C	100	0.192	31.7817	5.627	8.121	3.249	−0.015	2.813
150 °C	002	0.2362	34.3367	5.219	0.292	3.013	−7.255	2.609
250 °C	002	0.2362	34.3504	5.217	0.253	3.012	−7.291	2.608
350 °C	002	0.1968	34.3374	5.219	0.289	3.013	−7.257	2.609
450 °C	002	0.192	34.3518	5.217	0.249	3.012	−7.294	2.608
150 °C	101	0.1771	36.1749	4.962	−4.647	2.865	−11.821	2.481
250 °C	101	0.2362	36.1975	4.959	−4.704	2.863	−11.875	2.479
350 °C	101	5.204	3.249	4.963	−4.629	2.865	−11.805	2.481
450 °C	101	0.288	36.2056	4.958	−4.725	2.863	−11.894	2.479

The angle for a diffraction peak is defined as ϴ, where λ is the wavelength for the X-ray source in addition.

The strains ε_c and ε_a of the ZnO NPs generated at different calcination temperatures along various peaks of diffraction of the a-axis and c-axis, respectively, are taken into consideration because of the following equations [41], and the obtained results are summarized in Table 2.

$$\varepsilon_a = \frac{a - a_o}{a_o} \times 100\% \tag{8}$$

$$\varepsilon_c = \frac{c - c_o}{c_o} \times 100\% \tag{9}$$

There are unrestrained ZnO NPs everywhere a_o and c_o are designated as the standard lattice constants targeted in the database.

The inter-planar distance of biosynthesized ZnO NPs is significantly affected by changing the calcination temperature, as shown in Table 2, and it was investigated by using the following equation [42]:

$$\frac{1}{d^2} = \frac{4}{3} \left(\frac{h^2 + hk + k^2}{a^2} \right) + \frac{l^2}{c^2} \tag{10}$$

where h, k, and l are the Miller indices for the X-ray diffraction peaks.

The linear component of $(\alpha hv)^2$ versus h was extrapolated using transmittance spectra as shown in Figure 9, and the Tauc formula was used to determine the optical band-gap energy of ZnO NPs biosynthesized using thyme plant leaf extract at various calcination temperatures [43]:

$$(\alpha hv)^2 = A(hv - E_g)^n \tag{11}$$

where α is the absorption coefficient, hv is the photon energy, A is constant, E_g is the optical band-gap energy, and *n* depends on the kind of transmission (equals 1/2 for authorized

direct transmission). The transmittance spectrum is the primary focus of the α coefficient container, which is used in combination with [40].

$$\alpha = \frac{\ln\left(\frac{1}{T}\right)}{d} \tag{12}$$

where T is the transmittance for ZnO samples and d is the thickness of the sample.

3. Results and Discussion

3.1. Characterization of Thyme Plant Leaf Extract

The phytochemicals in the plant extract convert metal ions into metal nanoparticles. Consequently, the plant extract functions as both a reducing and stabilizing agent. UV-Vis spectroscopy was used to monitor the improvement of this reaction. Peak absorption was connected by the surface plasmon resonance (SPR) when electromagnetic waves interacted with conduction band oscillation of electrons in the spectrum of UV–visible spectroscopy, consequently replicating metal ion reduction and nanoparticle formation. Since there are many OH groups available for the creation of nanoparticles, Figure 2 demonstrates that the extract from thyme plant leaves consists of tannin, phenolic acids, flavonoids, and essential oils [32], which are regarded to be potential bio-reducing and stabilizing agents [44,45]. The main constituents of thyme [32] are flavonoids. These phytochemicals are particularly effective in reducing metal ions and stabilizing them in the nanoscale dimension because they are antioxidants and also devoid of harmful compounds. Additionally, they may offer nanoparticles of various shapes and sizes [46].
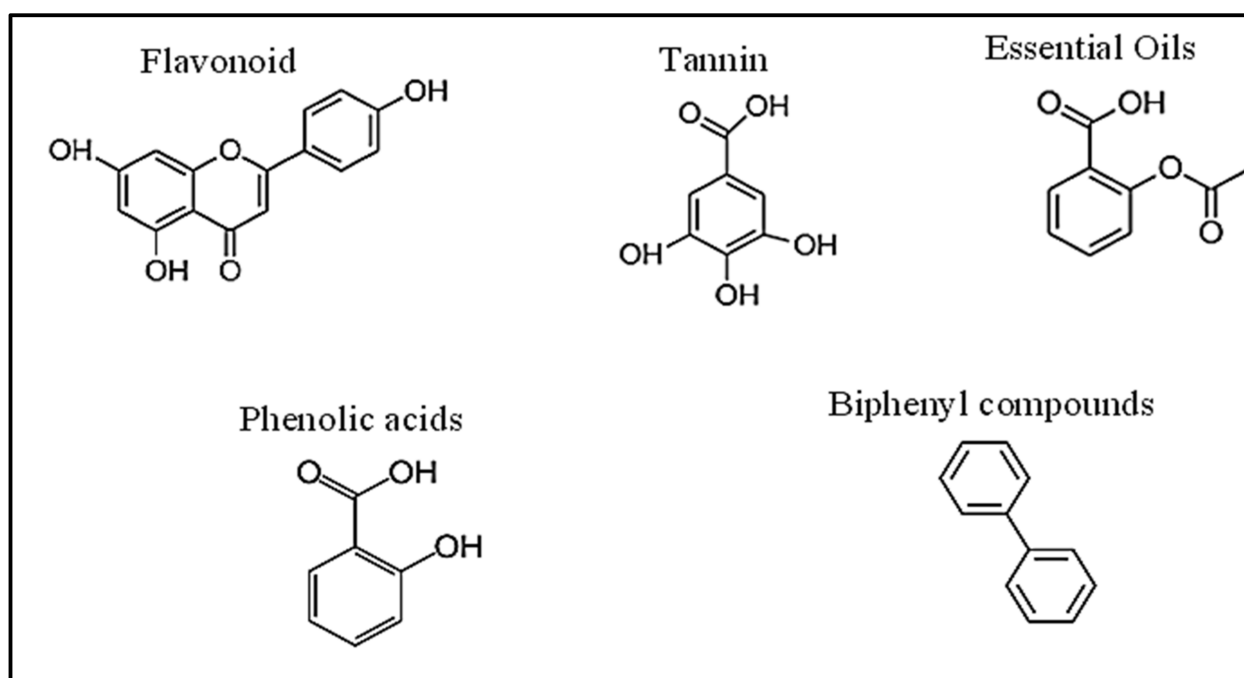

Figure 2. Available phytochemicals present in thyme plant leaves.

Figure 3 displays the thyme leaf extract's UV–visible spectrum. The spectrum's prominent and highest peaks, which are visible, are located at 266 nm and 313 nm, respectively. OH groups are a common stabilizing agent, a bio-reducing agent, the main phytochemical contained in the thyme plant's leaf extract, and perhaps the cause of the conspicuous peaks, and they may be used to produce nanoparticles [47]. Because they are antioxidants and free of hazardous substances, these phytochemicals are very efficient in reducing metal ions and keeping them in the nanoscale. Additionally, they can produce nanoparticles in a range of sizes and shapes [48]. The zinc ions combine to generate Zn (OH)2 through the

OH groups. There are three mechanisms at play: phase shift from Zn (OH)2 to ZnO, in situ crystallization, and reprecipitation of dissolution. Between-solids phase transition, the concept put forward by Wang et al. [46], is that water is removed from the lattice during the solid–solid phase transition.
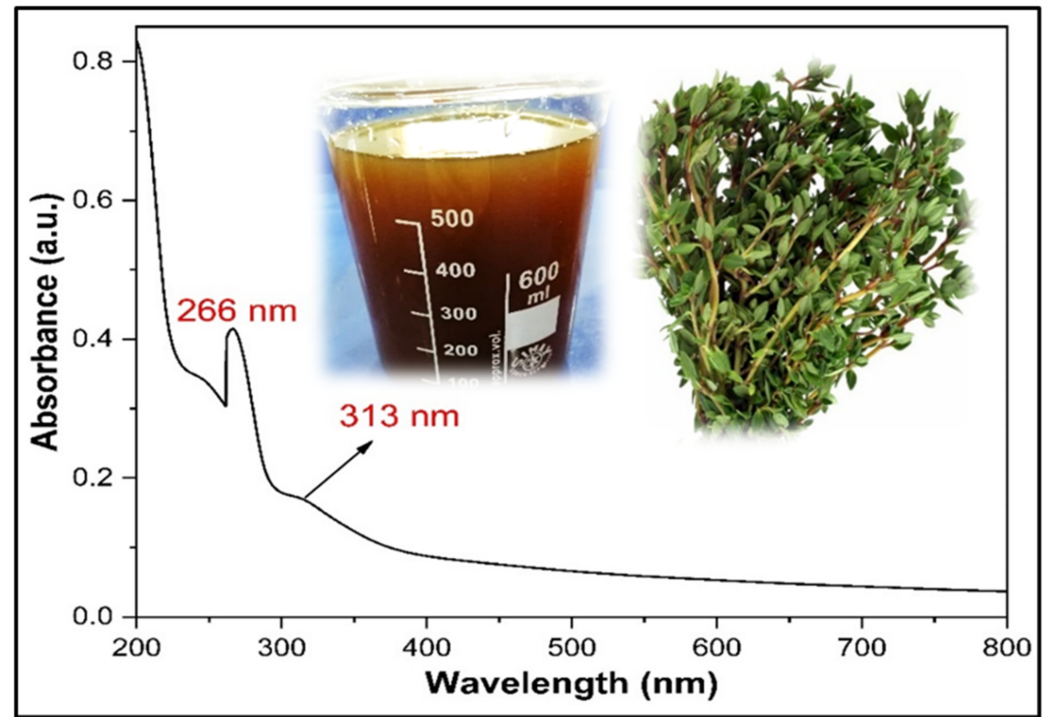

Figure 3. The UV–visible spectrum of leaf extracts of thyme plant.

By employing Fourier transform infrared (FTIR) spectra for ZnO NPs and plant extract, the functional groups associated with these reductive biomolecules in addition to the functional groups that aid in reducing ZnO generated by nanoparticles were considered [37,49].

Figure 4 depicts the FTIR spectrum for the thyme plant's leaf extract, which has many peaks that are discernible over the full range. Typically, the FTIR spectrum has two areas. Specifically, the 0–1500 cm^{-1} range contains the fingerprint region, while the 1800–4000 cm^{-1} range contains the functional group region. The FT-IR spectra provide details on the types of internal samples that are bonding with one another through numerous stages of matter [44,45,50]. The phyto-produced component of thyme plant leaf extract has a wavenumber range of 400–4000 cm^{-1} in the FT-IR spectra, as shown in Figure 4. The peak at 2929 cm^{-1} is due to methyl C-H asym./sym. stretching of methyl (−CH3), saturated aliphatic (alkene/alkyl); the peak at 1521 cm^{-1} is aromatic nitro compounds of nitrogen-oxy compounds, and another peak at 1411 cm^{-1} is vinyl C-H in-plane bending. However, one more peak at 1261 cm^{-1} is aromatic ethers, aryl -O stretching of ether, and oxy compound. Furthermore, the illustration of the graph reveals two peaks at 1056 and 1076 cm^{-1} that are primary amines and CN stretch. Moreover, the peak at 817 cm^{-1} is attributed to C-H 1,4-disubstitution (para) of C=C-C aromatic ring stretching. In addition, two other peaks at 777 cm^{-1} and 707 cm^{-1} are aliphatic chloro compounds, C-Cl stretch, and thiol or thioether, CH2-S- (C-S stretching). The final peak at 628 cm^{-1} is the alkyne C-H bending of acetylenic alkyne.

3.2. Characterization of ZnO Nanoparticles Synthesized by Green Method

Factors affecting the production of ZnO NPs include the quantity of plant extract or biomass present, the pH of the solution, the length of time needed for the reaction to complete, the reaction temperature, the calcination temperature, and the amount of present salt. To obtain the necessary shape and size of NPs for their maximal manipulation,

calibration of these growth components is crucial. This study looked at how different calcination temperatures affected the quality of the characteristics of ZnO nanoparticles [37]. Based on the results of the experiments, it is predicted that the biomolecules present in thyme leaf extract would interact chemically with zinc nitrate hexahydrate in the direction of producing ZnO NPs. However, owing to the extremely limited resources available in this area, the academic communities still face significant challenges in understanding the process of production and stability of nanoparticles made from plant extracts [37].
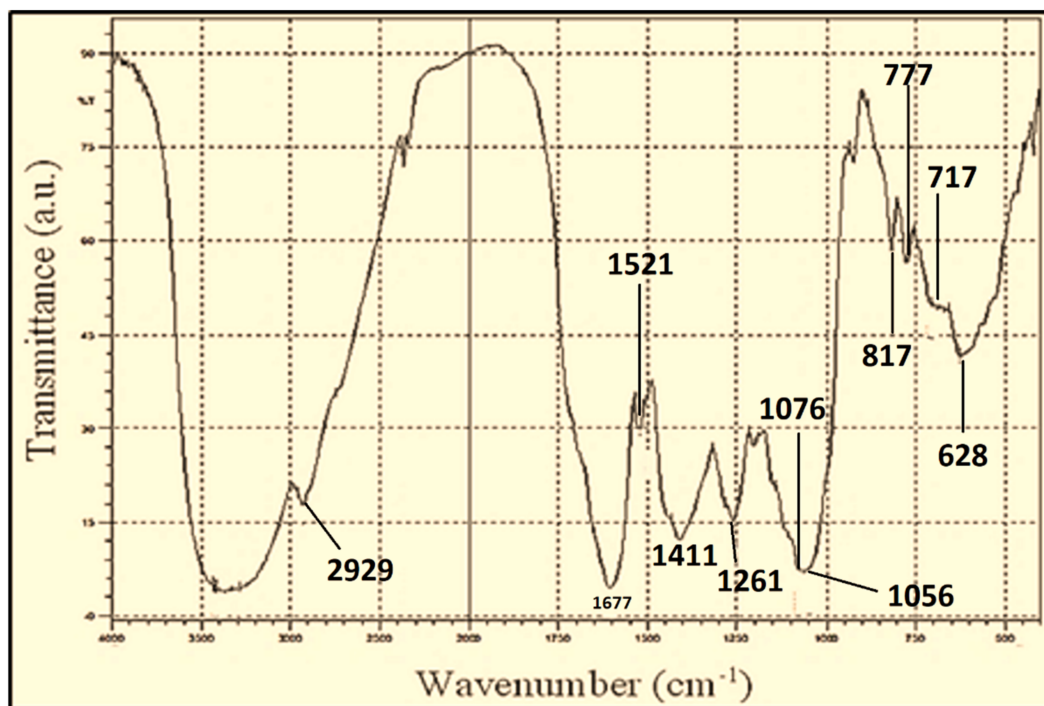
Figure 4. The FTIR spectrum of leaf extract of thyme plant.

To comprehend the process of NP formation, the majority of the research that is available focuses typically on the stabilizing and reducing agents that remain present in plant extracts. Many chemical substances have been used to create ZnO NPs; nevertheless, they are poisonous, corrosive, dangerous, very combustible, and neither environmentally friendly nor eco-friendly, and they might pose many health risks [51]. Accordingly, as a prospective replacement, phytochemicals that originate in plant extracts, such as those from leaves, fruits, peels, roots, flowers, seeds, and stems, should be researched. As reducing, capping, and stabilizing agents, these phytochemicals are essential and aimed at the production of nanoparticles [52]. However, in our situation, as a source aimed at metal ions, the combination was heated at an ideal temperature and for an ideal length of time. Typically, the aqueous plant extract is combined with a metal salt, for instance, zinc salt. To obtain the optimum yields, the variables pH, time, temperature, extract concentration, and salt should be regulated. It was experimentally demonstrated that ZnO NPs are unstable at 70 °C for 30 min since the biomolecules in thyme that remain present break down at this temperature, allowing ZnO NPs to mix and eventually producing bigger NPs. When ZnO is biosynthesized from plant extract, the pH of the mixture is one of the crucial factors impacting the characteristics of ZnO NPs [53]. Alkaline pH settings, or pH 8 and 9, are required, following the work of Alias et al., to create homogeneous particles with a good nanostructure and decreased agglomeration [54]. This claim is mostly supported by the technique we offer. We believe that agglomeration is caused by the acidic and neutral PHs of the Zn (OH)2 colloidal solutions throughout the biosynthetic process.

In other words, the combination contains enough OH- ions below pH 8 to demonstrate that ZnO NPs are produced more rapidly at basic pH than at acidic pH. Alkaline media show this by boosting surface plasmon resonance (SPR). The pH is increased as a result

of ionization of the OH groups in the plant extract biomolecules that aid in NP reduction. The number of metal particles in the mixture decreases during stirring and heating, and the color of the combination changes to brown or yellow, which is a reliable sign that nanoparticles are forming [38,55]. Even though this may be seen with the naked eye, further characterizing it still requires a UV-Vis spectrophotometer for validating the occurrence of nanoparticle formation using the aforementioned surface plasmon resonance (SPR) bands. Numerous phytochemicals, including biphenyl compounds, essential oils, flavonoids, tannin, and phenolic acids [32], are found in the extract of thyme leaves and are thought to have promise as bio-reducing and stabilizing agents. Without supplementary reducing agents or surfactants, the OH groups allow the synthesis of nanoparticles [37]. In reality, because various phytochemical agents react with metal ions in different ways, each plant extract generates nanoparticles in a variety of shapes, sizes, and crystallinities [56]. A positive indication that smaller particles are developing is the shift in color of the metal ion solution used in this study from clear to pale brown. As previously mentioned, the main chemical components of thyme are phenolic chemicals, mainly flavonoids. Thyme contains flavonoids, naturally occurring substances from the flavone family that include apigenin [57].

The main element on which we based our suggested strategy is as follows: Since ZnO NPs are created from an aqueous plant leaf extract, Figure 2 describes one of the possible procedures for the capping effect of the plant extract. When plant leaf extract is calcined in a stationary air environment, the complex compound formed by the Zn^{2+} cap and pre-existing phytochemicals undergoes direct breakdown, resulting in the generation of ZnO NPs. The procedures that were previously presented by Karnan and Selvakumar are well-aligned with our approach [58] and that of Jafarirad et al. [59]. A variety of hydroxyl (OH) groups extracted from thyme plant leaves have shown promise in the redox transformation of zinc ions (Zn^{+2}) into zero-valence zinc nanoparticles (Zn). Figure 2 shows how the supplied electrons can reduce the oxidized metal ions and create metallic nanoparticles. In the direction of the abundant hydroxyl, or OH, groups, the extract from thyme plant leaves complicatedly reacted with Zn^{+2} and reduced it to Zn^0. The generated Zn^0 was later brought back via the nucleation process. The growth process that followed this step resulted in the formation of nanoparticle clusters. The subsequent carboxylic acids (COOH) in the apigenin molecule were reduced, losing their hydrogen atom to create carboxylate ions (COO-). After that, the COO- and the remaining sequent were linked to the surface of the metal nanoparticles to function as a surfactant and stabilize the metal nanoparticles via electro-steric stabilization [30].

3.2.1. Field Emission Scanning Electron Microscopy (FESEM) Analysis

The top view of ZnO nanoparticles showing surface morphology produced by employing the green method and the extract from thyme plant leaves at numerous calcination temperatures is revealed in Figure 5. It reveals the orientation, size, shape, and density of the distribution of the nanoparticles. Figure 5 illustrates in what manner the calcination temperature exhibits a substantial impact on the shape, size, orientation, density, and surface morphology of ZnO NPs. As illustrated in Figure 5a, it was discovered that ZnO NPs were formed at lower calcination temperatures in place of seed layers or as non-orientation nanorods with high-density distributions in addition to an average size of around 39.4 nm. Following an increase in the calcination temperature to 250 °C, as seen in Figure 5b, the ZnO molecules progressively expanded and joined together to form semi-sphere-shaped ZnO nanoparticles with a non-uniform shape and an average particle size of 44.7 nm. As can be seen in Figure 5c, as the calcination temperature was increased to 350 °C, ZnO NPs exhibited a high rate of agglomeration with an average particle size of 51.23 nm. Additionally, they have a spherical form, a high-density distribution, and a variety of shapes and sizes. The better quality ZnO nanoparticles with accurate high-density distribution, uniform size, uniform shape, and spherical shape were produced at a higher calcination temperature of 450 °C, as revealed in Figure 5d. The typical particle size is 51.86 nm. As shown in

Figure 5, the majority of the synthesized ZnO NPs exhibited a highly spherical shape and were in the nanometer range. The generated ZnO NPs occasionally exhibited significant aggregation formation, which is characteristic of green synthesis nanoparticles. This is because biosynthetic NPs have a larger surface area, and their long-lasting affinities lead to their agglomeration or aggregation [21]. It might be argued that ecological variables have a great impact on NPs' stability and agglomeration. As a result, the NPs joined together as the nanoparticles developed and asymmetrical clusters spontaneously formed [60].
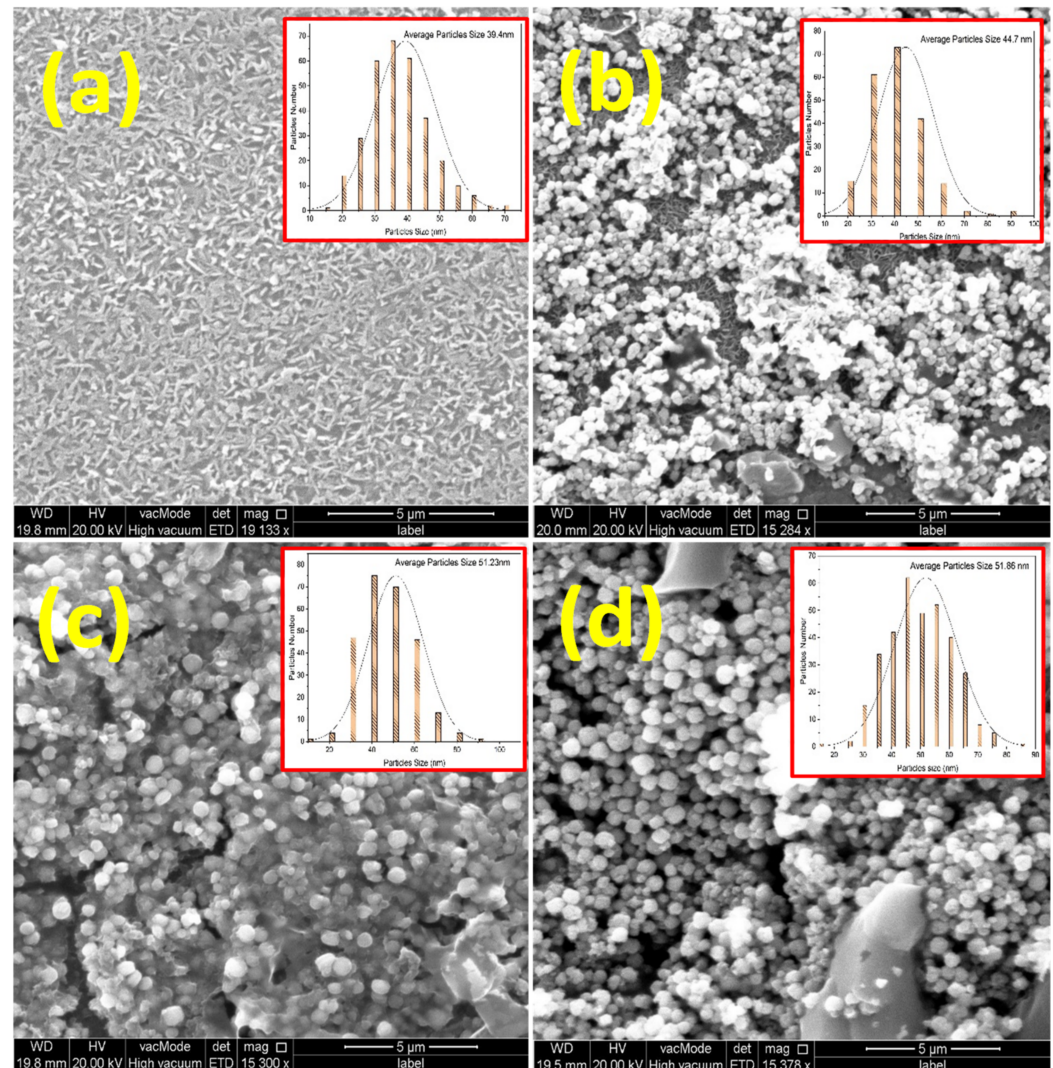
Figure 5. The FESEM top-view images of ZnO nanoparticles synthesized by using a green method and the leaf extract of the thyme plant at different calcination temperatures: (**a**) 150 °C, (**b**) 250 °C, (**c**) 350 °C, and (**d**) 450 °C.

3.2.2. Energy-Dispersive X-ray Spectroscopy (EDX) Analysis

The findings of an examination into the quantitative and qualitative chemical elements of the biosynthesized ZnO NPs formed via employing thyme plant leaf extract at various calcination temperatures are revealed in Figure 6 (150–450 °C). According to Figure 6, the investigation of the synthesized ZnO NP samples' EDX spectra showed that the primary chemical components of the samples were zinc (Zn), oxygen (O), and gold (Au). The existence of the Au might be attributed to the ZnO NP powder for all calcination temperatures applied throughout the FESEM imaging analysis to enhance the FESEM images. The EDX spectra showed two strong Zn peaks at 1 and 8.7 keV, respectively, as well as a single O signal at 0.5 keV, which is expected for ZnO NPs [61]. Strong Zn and O peak intensities in the sample were indicative of ZnO predominance. Additionally, it can be seen that

an EDX analysis of the produced ZnO NPs supports their high-purity chemical make-up. The atomic percent ratio of Zn:O in the NPs is almost 1:1, based on data from EDX and quantitative analysis.
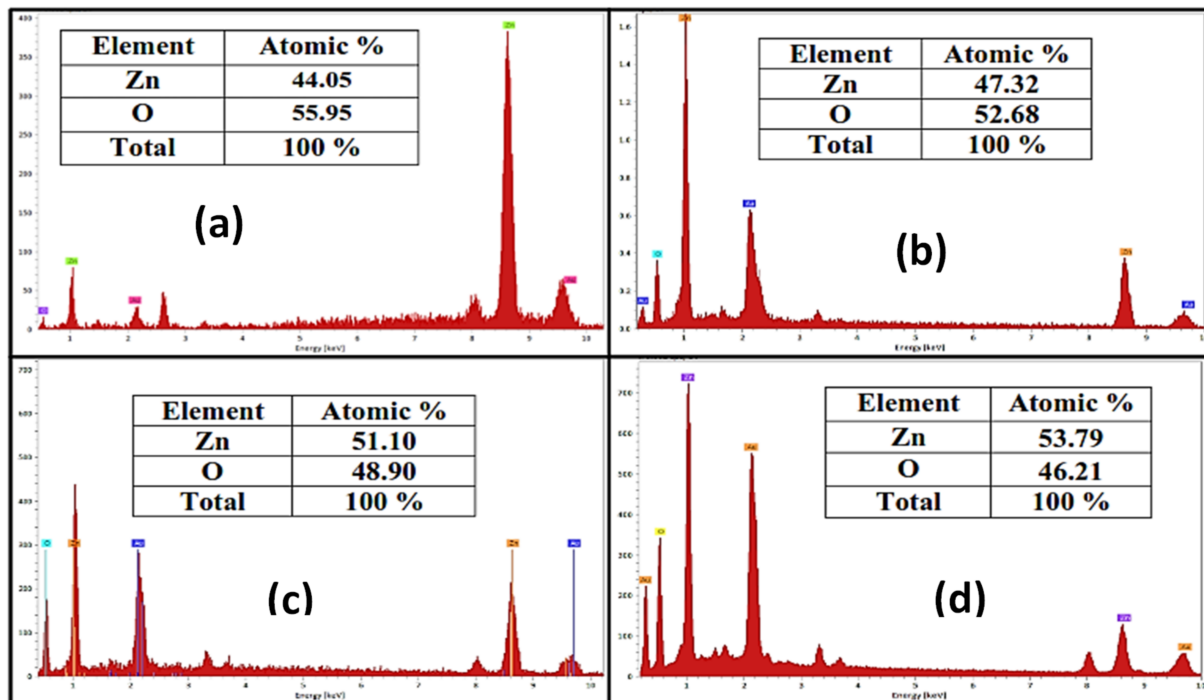

Figure 6. The EDX analysis of ZnO nanoparticles synthesized by using a green method and the leaf extract of the thyme plant at different calcination temperatures: (**a**) 150 °C, (**b**) 250 °C, (**c**) 350 °C, and (**d**) 450 °C.

3.2.3. X-ray Diffraction Analysis

The X-ray diffraction patterns of ZnO NPs created via the environmentally friendly method using thyme plant leaf extract at numerous calcination temperatures are revealed in Figure 7. The polycrystalline hexagonal crystal structure (wurtzite) of ZnO has been allocated to every XRD diffraction peak (JCPDS cards No. 98-018-5829). The lack of any further impurity- or defect-related diffraction peaks makes available additional evidence of the exceptional purity of the ZnO nanocrystals. Figure 7 and Table 2 demonstrate that altogether XRD patterns for all calcination temperatures exhibit the three strong and dominant peaks at (100), (002), and (101) with different values in addition to intensities. Growing calcination (annealing) temperature reinforced the polycrystalline hexagonal structure of the synthesized ZnO NPs, as shown by the fact that all higher peak intensities of ZnO NPs virtually increased with increasing calcination temperature [62]. All observed ZnO NP XRD patterns behavior for various calcination temperatures are in good accord with earlier studies [34,54,63].

By using the full width at half-maximum (FWHM) value for XRD spectra of ZnO NPs, the analysis of the crystal quality and compositional phase distribution of the formed ZnO NP hexagonal structure has been conducted. The value of FWHM of all plane peaks for all different calcination temperatures is significantly affected by the alteration in calcination temperature, as shown in Table 2. This demonstrates that changing the calcination temperature affects and enhances the quality of the crystal structure, which in turn affects the typical particle size of synthesized ZnO NPs.

For calcination temperatures of 150 °C, 250 °C, 350 °C, and 450 °C, the measured average particle size along diffraction peak (002) of biosynthesized ZnO NPs was 35.202 nm, 35.203 nm, 42.249 nm, and 43.308 nm, respectively. The average particle size increased along with the rise in calcination temperature. The increase in average particle size was

brought about by the reorientation of the particles generated by the heat energy employed during annealing, which also reduced the number of defects in grain boundaries [64]. The XRD results confirm the findings of the FESEM examination and the average particle size under investigation.
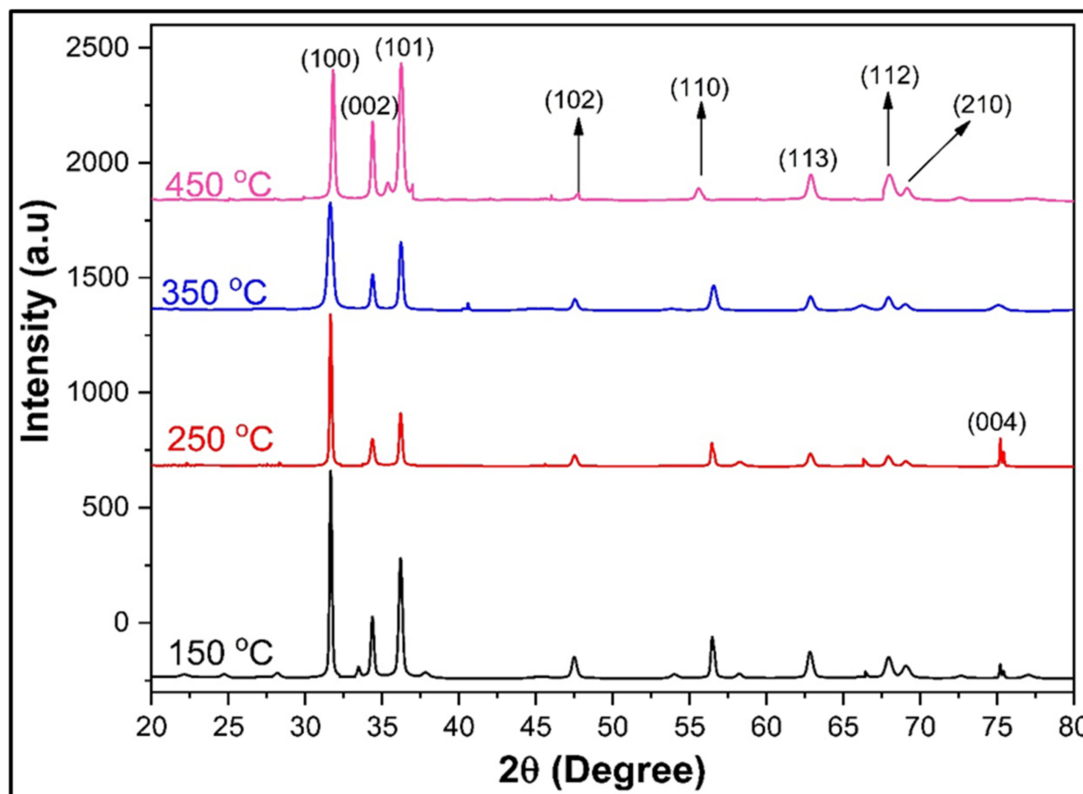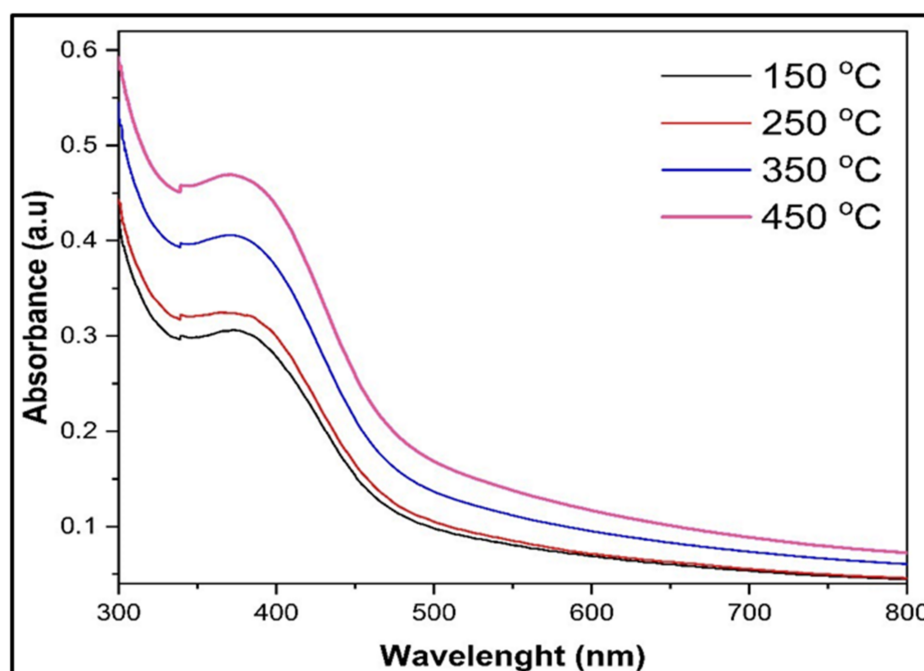

Figure 7. The XRD patterns of ZnO nanoparticles synthesized by using a green method and the leaf extract of the thyme plant at different calcination temperatures.

It should be noted that the variation in calcination temperature has a strong and considerable impact on the bond length and volume of ZnO NPs along all diffraction peaks. Because bond length and volume are both directly influenced by the lattice parameters a and c as well as the value of 2θ, the position of peak 2 amid numerous stronger diffraction peaks is unpredictable [40]. The structural features, intensity, lattice constants (a and c), peak position (θ), and internal strains (ε_c, ε_a) of ZnO NPs along the stronger three diffraction peaks (100), (002), and (101) are all broken down in Table 2 in detail.

As shown in Table 2, the differences between strains ε_c and ε_a originate from variations in inter-planar spacing values caused by an imbalance between substrate and crystal development. The variation in calcination temperature clearly and considerably affects the calculated lattice constants and strain along different peaks of diffraction, as shown in Table 2. There are also compressive and tensile stresses, as seen in Table 2. These strain values, which represent the lattice contraction and lattice constant expansion, respectively, are given as negative and positive strain values [39]. Using Bragg's law, the inter-planar distance of synthesized ZnO nanoparticles in conjunction with the three prominent and stronger diffraction peaks has been determined [39]. A summary of these findings is shown in Table 2. It can be demonstrated that the inter-planar distance of biosynthesized ZnO NPs is significantly affected by changing the calcination temperature.

3.2.4. Ultraviolet (UV)–Visible Spectroscopy Analysis

A UV-Vis spectroscopic study of the absorption spectrum in the range of wavelengths of 300–800 nm was used to determine the impact of different calcination temperatures on the optical characteristics of ZnO NPs made by using an extract from thyme plant

leaves, as shown in Figure 8. Figure 8 shows that the dominant (strong) feature of all ZnO NPs produced at different calcination temperatures is a high absorbance in the UV region below 400 nm and a low absorbance rate in the visible range. The results of the UV-Vis investigation are in excellent alignment with earlier research [42,62]. Low long-wavelength absorption values are caused by impurities in ZnO NP, such as oxygen vacancies that serve as donor defects and interstitial Zn atoms [43]. Additionally, for all calcination temperatures, the peak of absorption is pushed to a longer wavelength. Qualitatively, it is demonstrated that raising the calcination temperature lowered the band-gap energy [65]. However, the oxygen vacancy is connected to the closing band gap. We believe that the disordered crystal structure at the high calcination temperature was what created the oxygen vacancy in ZnO nanoparticles [66].

Figure 8. The UV–visible spectra of ZnO nanoparticles synthesized using a green method and the leaf extract of the thyme plant at different calcination temperatures.

Figure 9 demonstrates that the optical energy gap of the ZnO semiconductor, which corresponds to the straight transition band between the valance and conduction bands, is around 2.65 eV [67]. On the plot, at temperatures of 150 °C, 250 °C, 350 °C, and 450 °C, the band-gap energy of ZnO nanoparticles is around 2.7 eV, 2.6915 eV, 2.672 eV, and 2.645 eV, respectively. As some components of covering or modifying the surface with plant extract also reduce the band gap for the nanoparticles, a reduction in the band gap is still predicted as a result of utilizing the plant extract [68]. This discovery, which mostly applies to green nanoparticles, is not inconsistent with quantum confinement occurrences. When compared to nanoparticles created using traditional methods, biosynthesized ones are frequently more reactive [69]. Due to the reduced energy state separation, it is possible to relate the direction of particle reactivity in the quantum domain to the overall greater direction of a rise in electron populations in lower energy bands [70].

Metal NPs have diameters that are significantly smaller than visible light's wavelengths. They may absorb or disperse light depending on how they interact with it. Bulk metal oxides have a large band gap and little interaction potential. Their capacity to reflect and absorb energy, together with their increased sensitivity as they shrink, may affect how well they interact with one another. However, there is a link between the oxygen vacancy and the shrinking band gap. We think that the oxygen vacancy in ZnO nanoparticles was caused by the disordered crystal structure at the high calcination temperature [66].
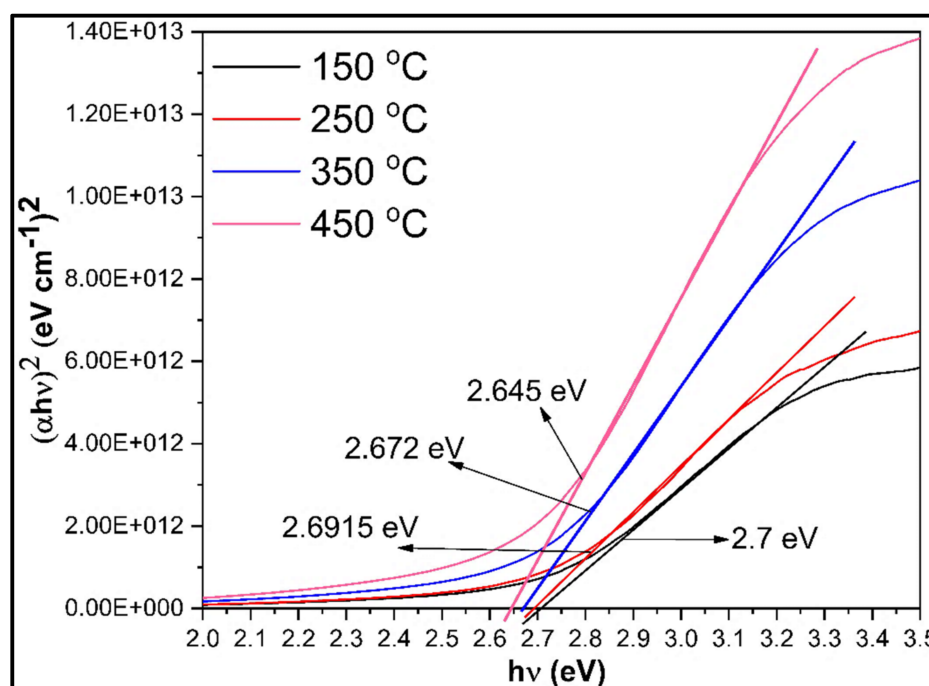
Figure 9. Tauc plot $(\alpha h\nu)^2$ versus energy band gap (hν) of ZnO nanoparticles synthesized by using a green method and the leaf extract of the thyme plant at different calcination temperatures.

3.2.5. The Fourier Transform Infrared Spectroscopy (FTIR) Analysis

The spectrum of FTIR was employed to examine the purity and composition for ZnO NPs produced via biosynthesis at different calcination temperatures, as shown in Figure 10. Figure 10 shows there was no discernible peak in the monitoring range that indicated the purity of the ZnO nanoparticles generated via using thyme leaf extract. The broad band at 620 cm^{-1} disappeared for the ZnO nanoparticles synthesized. An additional peak was generated at 421 cm^{-1} for ZnO nanoparticles formed as a result of this process, representing bonding vibrations of zinc and oxygen [71]. The FTIR spectrum of ZnO NPs produced at 150 °C is shown in Figure 10a. A broad absorption peak in the range of 3000–3500 cm^{-1} is present in both figures, which can be attributed to the characteristic absorption of 3506 cm^{-1}, representing dimeric OH stretching, and 3448 cm^{-1}, 3431 cm^{-1}, and 3414 cm^{-1}, representing hydroxy group H-bonded OH stretching. In addition, in the range between 1500 and 2000 cm^{-1}, the presence of the absorption peak at 1776 cm^{-1} is attributed to the acid (asyl) halide of the carbonyl compound, and the peak at 1544 cm^{-1} is attributed to the aliphatic nitro compound. However, peaks at 1384 cm^{-1} are due to phenol or tertiary alcohol, OH bending. In addition, the peak in the range of 1273 cm^{-1} is due to the presence of organic nitrate in the simple hetero-oxy compound. However, another peak found at 1155 cm^{-1} is attributed to tertiary amine or CN stretching; other peaks detected at 1072 cm^{-1} are cyclic ethers, large rings, and C-O stretching. Furthermore, the peak in the range of 400–100cm^{-1}, at 879, 852, and 825 cm^{-1} is peroxide C-O-O- stretching from the ether oxy compound. In addition, the peak at 702 cm^{-1} is aliphatic chloro compound, C-Cl stretching. Likewise, another two peaks are noticed: the peak at 474 cm^{-1} is polysulfide S-S stretching, and the peak at 437 cm^{-1} is aryl disulfide S-S stretching.

The FTIR spectrum of ZnO NPs biosynthesized at 250 °C is shown in Figure 10b. As we already stated, the absorption peak at 3441 cm^{-1} is the hydroxy group H-bonded OH stretching. In addition, another peak found at 1616 cm^{-1} is due to alkenyl C=C stretching, and the peak 1122 cm^{-1} is due to aliphatic fluoro compounds, C-F stretching. However, one more peak at 991 cm^{-1} is attributable to silicate ions of common inorganic ions. Furthermore, the final absorption peak at 617 cm^{-1} is the disulfide S-S stretching. In addition, the FTIR spectrum of ZnO NPs biosynthesized at 350 °C is shown in Figure 10c. The broad peak at 3508 cm^{-1} corresponds to dimeric OH stretching, and another peak

at 1627 cm^{-1} is due to alkenyl C=C stretching. However, one more peak at 1116 cm^{-1} is due to cyclic ethers, large rings, and C-O stretching. An additional peak at 991 cm^{-1} is attributable to silicate ions of common inorganic ions. Additionally, the final absorption peak at 617 cm^{-1} is the disulfide S-S stretching. The final peak detected at 449 cm^{-1} is aryl disulfide S-S stretching.
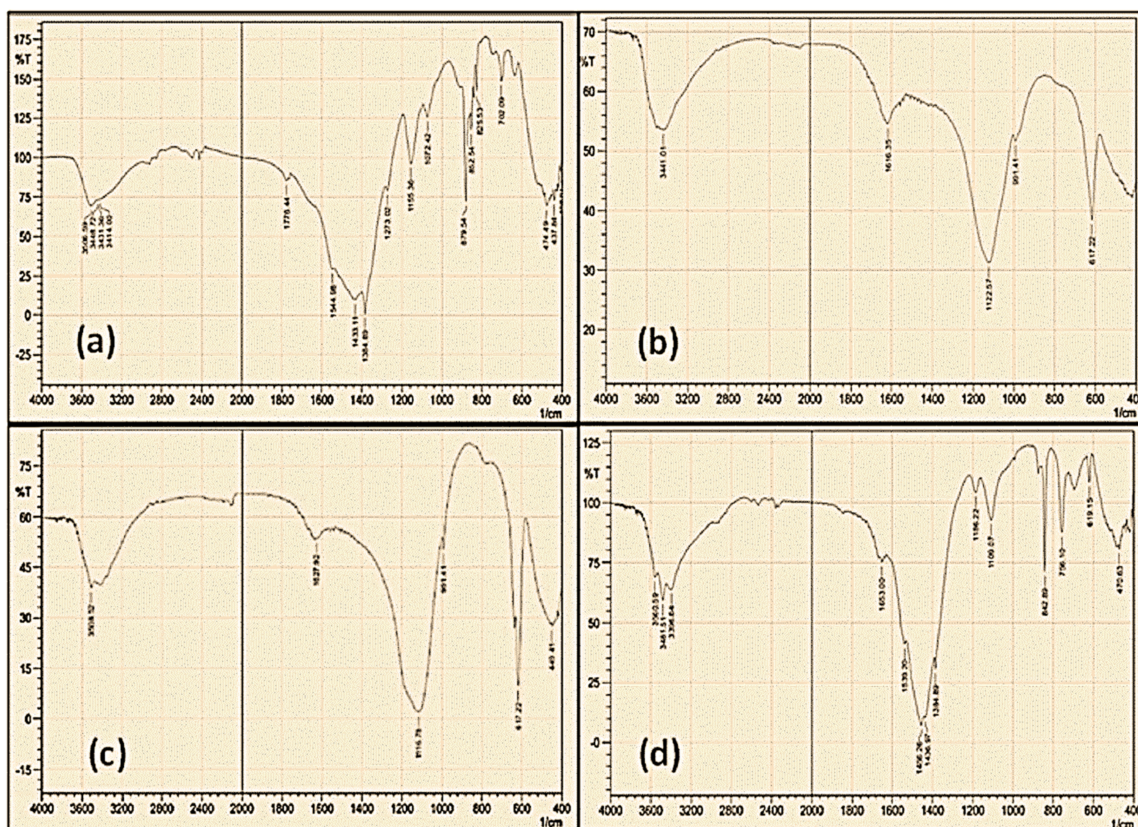

Figure 10. The FTIR spectra of ZnO nanoparticles synthesized by using a green method and the leaf extract of the thyme plant at different calcination temperatures: (**a**) 150 °C, (**b**) 250 °C, (**c**) 350 °C, and (**d**) 450 °C.

In addition, the FTIR spectrum of ZnO NPs biosynthesized at 450 °C is shown in Figure 10d. The areas that had the most significant absorption peaks at 3560, 3481, and 3396 cm^{-1} are the hydroxyl group, H-bonded OH stretching of alcohol, and hydroxy compound. In addition, another two peaks in the region (1653 cm^{-1} and 1539 cm^{-1}) are secondary amine, >N-H bending of secondary amine. However, the peaks at 1456 cm^{-1} and 1436 cm^{-1} are methyl C-H asym./sym. stretching. Furthermore, one more peak at 1384 cm^{-1} is phenol or tertiary alcohol, OH bending. Additionally, the other two peaks at 1186 cm^{-1} and 1109 cm^{-1} are due to aromatic C-H in-plane bending. Moreover, the peak at 842 cm^{-1} is due to C-H 1,4-disubstitution (para) of the aromatic ring. Likewise, two other peaks at 756 cm^{-1} and 619 cm^{-1} are a result of the disulfides (C-S stretching) of thiols and thio-substituted compounds. A final peak at 470 cm^{-1} is polysulfide S-S stretching.

4. Conclusions

Zinc oxide nanoparticles with high quality have been fabricated successfully by employing a green method using the leaf extract of the thyme plant. The effects of the different calcination temperatures on the production properties such as morphology, shape, size, orientation, distribution, crystal structure quality, optical properties, and chemical composition of ZnO NPs have been studied in detail. The results revealed that the leaf extract of the thyme plant is a very good choice for the fabrication of ZnO NPs by the green method. In addition, the results showed that the variation in calcination temperature has

an important and strong impact on the shape, average size, morphology, crystal quality, optical properties, and energy band gap of ZnO NPs. The FESEM result shows the average size of ZnO NPs was increased from 39.4 nm to 51.86 nm with an increase in the calcination temperature from 150 °C to 450 °C. The calcination temperature has a great effect on the crystal size and quality for the hexagonal wurtzite structure of ZnO NPs, and the particle size was increased from 35.202 nm to 43.30 nm with an increase in calcination temperature. In addition, the FTIR analysis results at different calcination temperatures confirm that the ZnO NPs were synthesized with high purity from thyme plant leaf extract. In addition, high absorbance was shown below 400 nm in the UV region, and the visible range had a low absorbance rate. The energy band gap was decreased from 2.7 nm to 2.645 nm with an increase in calcination temperature. Our findings support the use of thyme plant leaf extraction for the production of ZnO NPs in a quick, simple, and environmentally friendly manner. The effect of the difference in calcination temperatures on ZnO NP quality was investigated and the optimum calcination temperature for the green synthesis of ZnO NPs was identified. According to the results obtained for the biosynthesized ZnO NPs, the ZnO NPs biosynthesized at the calcination temperature of 450 °C showed a high quality and improvement compared to the ZnO NPs synthesized at other calcination temperatures. In addition, the novelty of this study is the green synthesis of ZnO nanoparticles from thyme plant leaf extract, which might be used for photocatalysis, water pollution removal, medicinal (antibacterial) applications, solar cells, and cosmetic applications.

References

1. Tabrez, S.; Musarrat, J.; Al-khedhairy, A.A. Countering drug resistance, infectious diseases, and sepsis using metal and metal oxides nanoparticles: Current status. *Colloids Surf. B Biointerfaces* **2016**, *146*, 70–83.
2. Sastry, M.; Ahmad, A.; Islam Khan, M.; Kumar, R. Biosynthesis of metal nanoparticles using fungi and actinomycete. *Curr. Sci.* **2003**, *85*, 162–170.
3. Rao, M.D.; Gautam, P. Synthesis and characterization of ZnO nanoflowers using *Chlamydomonas reinhardtii*: A green approach. *Environ. Prog. Sustain. Energy* **2016**, *35*, 1020–1026. [CrossRef]
4. Nasrollahzadeh, M.; Sajjadi, M.; Sajadi, S.M.; Issaabadi, Z. Green Nanotechnology. *Interface Sci. Technol.* **2019**, *28*, 145–198. [CrossRef]
5. Jayaseelan, C.; Rahuman, A.A.; Kirthi, A.V.; Marimuthu, S.; Santhoshkumar, T.; Bagavan, A.; Gaurav, K.; Karthik, L.; Rao, K.B. Novel microbial route to synthesize ZnO nanoparticles using *Aeromonas hydrophila* and their activity against pathogenic bacteria and fungi. *Spectrochim. Acta A Mol. Biomol. Spectrosc.* **2012**, *90*, 78–84. [CrossRef]
6. Abdulrahman, A.F. The effect of different substrate-inclined angles on the characteristic properties of ZnO nanorods for UV photodetectors applications. *J. Mater. Sci. Mater. Electron.* **2020**, *31*, 14357–14374. [CrossRef]

7. Dobrucka, R.; Długaszewska, J. Biosynthesis and antibacterial activity of ZnO nanoparticles using *Trifolium pratense* flower extract. *Saudi J. Biol. Sci.* **2015**, *23*, 517–523. [CrossRef]

8. Anbuvannan, M.; Ramesh, M.; Viruthagiri, G.; Shanmugam, N.; Kannadasan, N. Synthesis, characterization and photocatalytic activity of ZnO nanoparticles prepared by biological method. *Spectrochim. Acta A Mol. Biomol. Spectrosc.* **2015**, *143*, 304–308. [CrossRef]

9. Abdulrahman, A.F. The Influence of Various Reactants in the Growth Solution on the Morphological and Structural Properties of ZnO Nanorods. *Passer J. Basic Appl. Sci.* **2020**, *2*, 69–75. [CrossRef]

10. Efa, M.T.; Imae, T. Effects of carbon dots on ZnO nanoparticle-based dye-sensitized solar cells. *Electrochim. Acta* **2019**, *303*, 204–210. [CrossRef]

11. Sundrarajan, M.; Ambika, S.; Bharathi, K. Plant-extract mediated synthesis of ZnO nanoparticles using *Pongamia pinnata* and their activity against pathogenic bacteria. *Adv. Powder Technol.* **2015**, *26*, 1294–1299. [CrossRef]

12. Vanathi, P.; Rajiv, P.; Narendhran, S.; Rajeshwari, S.; Rahman, P.K.; Venckatesh, R. Biosynthesis and characterization of phyto mediated zinc oxide nanoparticles: A green chemistry approach. *Mater. Lett.* **2014**, *134*, 13–15. [CrossRef]

13. Abdulrahman, A.F.; Ahmed, S.M.; Hamad, S.M.; Barzinjy, A.A. Effect of Growth Temperature on Morphological, Structural, and Optical Properties of ZnO Nanorods Using Modified Chemical Bath Deposition Method. *J. Electron. Mater.* **2021**, *50*, 1482–1495. [CrossRef]

14. Huang, W.; Tao, F.; Li, F.; Mortimer, M.; Guo, L.-H. Antibacterial nanomaterials for environmental and consumer product applications. *NanoImpact* **2020**, *20*, 100268. [CrossRef]

15. Rambabu, K.; Bharath, G.; Banat, F.; Show, P.L. Green synthesis of zinc oxide nanoparticles using *Phoenix dactylifera* waste as bioreductant for effective dye degradation and antibacterial performance in wastewater treatment. *J. Hazard. Mater.* **2021**, *402*, 123560. [CrossRef] [PubMed]

16. Jamdagni, P.; Khatri, P.; Rana, J.S. Green synthesis of zinc oxide nanoparticles using flower extract of *Nyctanthes arbor-tristis* and their antifungal activity. *J. King Saud Univ.-Sci.* **2018**, *30*, 168–175. [CrossRef]

17. Prasad, K.; Jha, A.K. ZnO Nanoparticles: Synthesis and Adsorption Study. *Nat. Sci.* **2009**, *01*, 129–135. [CrossRef]

18. Chauhan, A.; Verma, R.; Kumari, S.; Sharma, A.; Shandilya, P.; Li, X.; Batoo, K.M.; Imran, A.; Kulshrestha, S.; Kumar, R. Photocatalytic dye degradation and antimicrobial activities of Pure and Ag-doped ZnO using *Cannabis sativa* leaf extract. *Sci. Rep.* **2020**, *10*, 7881. [CrossRef]

19. Bhushan, B.; Jahan, K.; Verma, V.; Murty, B.; Mondal, K. Photodegradation of methylene blue dye by powders of Ni–ZnO floweret consisting of petals of ZnO nanorod around Ni-rich core. *Mater. Chem. Phys.* **2020**, *253*, 123394. [CrossRef]

20. Aldeen, T.S.; Mohamed, H.E.A.; Maaza, M. ZnO nanoparticles prepared via a green synthesis approach: Physical properties, photocatalytic and antibacterial activity. *J. Phys. Chem. Solids* **2022**, *160*, 110313. [CrossRef]

21. Vidya, C.; Hiremath, S.; Chandraprabha, M.N.; Antonyraj, M.L.; Gopal, I.V.; Jain, A.; Bansal, K. Green synthesis of ZnO nanoparticles by *Calotropis gigantea*. *Int. J. Curr. Eng. Technol.* **2013**, *1*, 118–120.

22. Aladpoosh, R.; Montazer, M. The role of cellulosic chains of cotton in biosynthesis of ZnO nanorods producing multifunctional properties: Mechanism, characterizations and features. *Carbohydr. Polym.* **2015**, *126*, 122–129. [CrossRef] [PubMed]

23. Chung, I.-M.; Park, I.; Seung-Hyun, K.; Thiruvengadam, M.; Rajakumar, G. Plant-Mediated Synthesis of Silver Nanoparticles: Their Characteristic Properties and Therapeutic Applications. *Nanoscale Res. Lett.* **2016**, *11*, 40. [CrossRef] [PubMed]

24. Singh, J.; Dutta, T.; Kim, K.-H.; Rawat, M.; Samddar, P.; Kumar, P. 'Green' synthesis of metals and their oxide nanoparticles: Applications for environmental remediation. *J. Nanobiotechnol.* **2018**, *16*, 84. [CrossRef] [PubMed]

25. Karthik, L.; Vishnu Kirthi, A.; Ranjan, S.; Mohana Srinivasan, V. (Eds.) *Biological Synthesis of Nanoparticles and Their Applications*, 1st ed.; CRC Press: Boca Raton, FL, USA, 2020. [CrossRef]

26. Mohammad Inejad, R.; Karimi, S.; Iravani, S.; Varma, R.S. Plant-derived nanostructures: Types and applications. *Green Chem.* **2015**, *18*, 20–52. [CrossRef]

27. Heinlaan, M.; Ivask, A.; Blinova, I.; Dubourguier, H.C.; Kahru, A. Toxicity of nano-sized and bulk ZnO, CuO and TiO2 to bacteria Vibrio fischeri and crustaceans Daphnia magna and Thamnocephalus platyurus. *Chemosphere* **2008**, *71*, 1308–1316. [CrossRef]

28. Gnanajobitha, G.; Paulkumar, K.; Vanaja, M.; RajeshKumar, S.; Malarkodi, C.; Annadurai, G.; Kannan, C. Fruit-mediated synthesis of silver nanoparticles using *Vitis vinifera* and evaluation of their antimicrobial efficacy. *J. Nanostruct. Chem.* **2013**, *3*, 67. [CrossRef]

29. Qu, J.; Yuan, X.; Wang, X.; Shao, P. Zinc accumulation and synthesis of ZnO nanoparticles using *Physalis alkekengi* L. *Environ. Pollut.* **2011**, *159*, 1783–1788. [CrossRef]

30. Agarwal, H.; Kumar, S.V.; Rajeshkumar, S. A review on green synthesis of zinc oxide nanoparticles—An eco-friendly approach. *Resour.-Efficient Technol.* **2017**, *3*, 406–413. [CrossRef]

31. Sackey, J.; Nwanya, A.; Bashir, A.; Matinise, N.; Ngilirabanga, J.; Ameh, A.; Coetsee, E.; Maaza, M. Electrochemical properties of *Euphorbia pulcherrima* mediated copper oxide nanoparticles. *Mater. Chem. Phys.* **2020**, *244*, 122714. [CrossRef]

32. Nieto, G. A Review on Applications and Uses of *Thymus* in the Food Industry. *Plants* **2020**, *9*, 961. [CrossRef] [PubMed]

33. Thi, T.U.D.; Nguyen, T.T.; Thi, Y.D.; Thi, K.H.T.; Phan, B.T.; Pham, K.N. Green synthesis of ZnO nanoparticles using orange fruit peel extract for antibacterial activities. *RSC Adv.* **2020**, *10*, 23899.

34. Iwan, S.; Zhao, J.; Tan, S.; Sun, X. Enhancement of UV photoluminescence in ZnO tubes grown by metal organic chemical vapour deposition (MOCVD). *Vacuum* **2018**, *155*, 408–411. [CrossRef]

35. Mohar, R.S.; Iwan, S.; Djuhana, D.; Imawan, C.; Harmoko, A.; Fauzia, V. Post-annealing effect on optical absorbance of hydrothermally grown zinc oxide nanorods. In Proceedings of the AIP Conference—1st International Symposium on Current Progress in Mathematics and Sciences, Depok, Indonesia, 3–4 November 2015; Volume 1729.

36. Iwan, S.; Fauzia, V.; Umar, A.A.; Sun, X.W. Room temperature photoluminescence properties of ZnO nanorods grown by hydrothermal reaction. In Proceedings of the AIP Conference—1st International Symposium on Current Progress in Mathematics and Sciences, Depok, Indonesia, 3–4 November 2015; Volume 1729.

37. Barzinjy, A.A.; Hamad, S.M.; Abdulrahman, A.F.; Biro, S.J.; Ghafor, A.A. Biosynthesis, Characterization and Mechanism of Formation of ZnO Nanoparticles Using *Petroselinum crispum* Leaf Extract. *Curr. Org. Synth.* **2020**, *17*, 558–566. [CrossRef]

38. Barzinjy, A.A.; Azeez, H.H. Green synthesis and characterization of zinc oxide nanoparticles using *Eucalyptus globulus* Labill. leaf extract and zinc nitrate hexahydrate salt. *SN Appl. Sci.* **2020**, *2*, 991. [CrossRef]

39. Sharma, V. A Review on Characterization of Solid Dispersion. *Int. J. Eng. Appl. Sci. Technol.* **2019**, *4*, 127–128. [CrossRef]

40. Abdulrahman, A.; Ahmed, S.; Barzinjy, A.; Hamad, S.; Ahmed, N.; Almessiere, M. Fabrication and Characterization of High-Quality UV Photodetectors Based ZnO Nanorods Using Traditional and Modified Chemical Bath Deposition Methods. *Nanomaterials* **2021**, *11*, 677. [CrossRef] [PubMed]

41. Abdulrahman, A.F.; Abd-Alghafour, N. Synthesis and characterization of ZnO nanoflowers by using simple spray pyrolysis technique. *Solid-State Electron.* **2022**, *189*, 108225. [CrossRef]

42. Ashraf, R.; Riaz, S.; Kayani, Z.N.; Naseem, S. Effect of Calcination on properties of ZnO nanoparticles. *Mater. Today Proc.* **2015**, *2*, 5468–5472. [CrossRef]

43. Shabannia, R.; Abu Hassan, H. Characteristics of photoconductive UV photodetector based on ZnO nanorods grown on polyethylene naphthalate substrate by chemical bath deposition method. *Electron. Mater. Lett.* **2014**, *10*, 837–843. [CrossRef]

44. Srivastava, V.; Gusain, D.; Sharma, Y.C. Synthesis, characterization and application of zinc oxide nanoparticles (n-ZnO). *Ceram. Int.* **2013**, *39*, 9803–9808. [CrossRef]

45. Zandi, S.; Kameli, P.; Salamati, H.; Ahmadvand, H.; Hakimi, M. Microstructure and optical properties of ZnO nanoparticles prepared by a simple method. *Phys. B Condens. Matter* **2011**, *406*, 3215–3218. [CrossRef]

46. Ovais, M.; Khalil, A.T.; Raza, A.; Khan, M.A.; Ahmad, I.; Islam, N.U.; Saravanan, M.; Ubaid, M.F.; Ali, M.; Shinwari, Z.K. Green synthesis of silver nanoparticles via plant extracts: Beginning a new era in cancer theranostics. *Nanomedicine* **2016**, *11*, 3157–3177. [CrossRef]

47. Singh, P.; Kim, Y.-J.; Zhang, D.; Yang, D.-C. Biological Synthesis of Nanoparticles from Plants and Microorganisms. *Trends Biotechnol.* **2016**, *34*, 588–599. [CrossRef] [PubMed]

48. Hocine, R.; Mazauric, J.; Madani, K.; Boulekbache-Makhlouf, L. Phytochemical analysis and antioxidant activity of *Eucalyptus globulus*: A comparative study between fruits and leaves extracts. *J. Chem. Eng. Bioanal. Chem.* **2016**, *1*, 23–29.

49. Norouzi, R.; Hejazy, M.; Ataei, A. Scolicidal effect of zinc oxide nanoparticles against hydatid cyst protoscolices in vitro. *Nanomed. Res. J.* **2019**, *4*, 23–28. [CrossRef]

50. Mittal, A.K.; Chisti, Y.; Banerjee, U.C. Synthesis of metallic nanoparticles using plant extracts. *Biotechnol. Adv.* **2013**, *31*, 346–356. [CrossRef]

51. Ahmed, S.; Annu; Chaudhry, S.A.; Ikram, S. A review on biogenic synthesis of ZnO nanoparticles using plant extracts and microbes: A prospect towards green chemistry. *J. Photochem. Photobiol. B* **2017**, *166*, 272–284. [CrossRef]

52. Wahab, R.; Ansari, S.A.; Kim, Y.S.; Song, M.; Shin, H.-S. The role of pH variation on the growth of zinc oxide nanostructures. *Appl. Surf. Sci.* **2009**, *255*, 4891–4896. [CrossRef]

53. Alias, S.; Ismail, A.; Mohamad, A. Effect of pH on ZnO nanoparticle properties synthesized by sol–gel centrifugation. *J. Alloys Compd.* **2010**, *499*, 231–237. [CrossRef]

54. Ochieng, P. Green route synthesis and characterization of ZnO nanoparticles using *Spathodea campanulata*. *Int. J. Biochem. Phys.* **2015**, *23*, 53–61.

55. Rajeshkumar, S. Anticancer and enhanced antimicrobial activity of biosynthesizd silver nanoparticles against clinical pathogens. *J. Mol. Struct.* **2016**, *1116*, 165–173. [CrossRef]

56. Farzaei, M.H.; Abbasabadi, Z.; Ardekani, M.R.; Rahimi, R.; Farzaei, F. Parsley: A review of ethnopharmacology, phytochemistry and biological activities. *J. Tradit. Chin. Med.* **2013**, *33*, 815–826. [CrossRef]

57. Karnan, T.; Selvakumar, S.A.S. Biosynthesis of ZnO nanoparticles using rambutan (*Nephelium lappaceum* L.) peel extract and their photocatalytic activity on methyl orange dye. *J. Mol. Struct.* **2016**, *1125*, 358–365. [CrossRef]

58. Jafarirad, S.; Mehrabi, M.; Divband, B.; Kosari-Nasab, M. Biofabrication of zinc oxide nanoparticles using fruit extract of *Rosa canina* and their toxic potential against bacteria: A mechanistic approach. *Mater. Sci. Eng. C* **2016**, *59*, 296–302. [CrossRef]

59. Basnet, P.; Chanu, T.I.; Samanta, D.; Chatterjee, S. A review on bio-synthesized zinc oxide nanoparticles using plant extracts as reductants and stabilizing agents. *J. Photochem. Photobiol. B Biol.* **2018**, *183*, 201–221. [CrossRef]

60. Shim, Y.J. Zinc oxide nanoparticles synthesized by *Suaeda japonica* Makino and their photocatalytic degradation of methylene blue. *Optik* **2019**, *182*, 1015–1020. [CrossRef]

61. Sugihartono, I.; Retnoningtyas, A.; Rustana, C.; Umiatin; Yudasari, N.; Isnaeni; Imawan, C.; Kurniadewi, F. The influence of calcination temperature on optical properties of ZnO nanoparticles. In Proceedings of the AIP Conference—The 8th National Physics Seminar, Jakarta, Indonesia, 29–30 June 2019. [CrossRef]

62. Zak, A.K.; Abrishami, M.E.; Majid, W.A.; Yousefi, R.; Hosseini, S.M. Effects of annealing temperature on some structural and optical properties of ZnO nanoparticles prepared by a modified sol–gel combustion method. *Ceram. Int.* **2011**, *37*, 393–398. [CrossRef]

63. Abdulrahman, A.F.; Ahmed, S.M.; Hamad, S.M.; Almessiere, M.A.; Ahmed, N.M.; Sajadi, S.M. Effect of different pH values on growth solutions for the ZnO nanostructures. *Chin. J. Phys.* **2021**, *71*, 175–189. [CrossRef]

64. Korake, P.; Dhabbe, R.; Kadam, A.; Gaikwad, Y.; Garadkar, K. Highly active lanthanum doped ZnO nanorods for photodegradation of metasystox. *J. Photochem. Photobiol. B Biol.* **2014**, *130*, 11–19. [CrossRef]

65. Wang, J.; Wang, Z.; Huang, B.; Ma, Y.; Liu, Y.; Qin, X.; Zhang, X.; Dai, Y. Oxygen Vacancy Induced Band-Gap Narrowing and Enhanced Visible Light Photocatalytic Activity of ZnO. *ACS Appl. Mater. Interfaces* **2012**, *4*, 4024–4030. [CrossRef] [PubMed]

66. Roza, L.; Rahman, M.Y.A.; Umar, A.A.; Salleh, M.M. Direct growth of oriented ZnO nanotubes by self-selective etching at lower temperature for photo-electrochemical (PEC) solar cell application. *J. Alloys Compd.* **2015**, *618*, 153. [CrossRef]

67. Khan, M.M.; Saadah, N.H.; Harunsani, M.H.; Tan, A.L.; Cho, M.H. Potentials of Costus woodsonii leaf extract in producing narrow band gap ZnO nanoparticles. *Mater. Sci. Semicond. Process.* **2019**, *91*, 194–200. [CrossRef]

68. Pantidos, N.; Horsfall, L.E. Biological synthesis of metallic nanoparticles by bacteria, fungi and plants. *J. Nanomed. Nanotechnol.* **2014**, *5*, 1. [CrossRef]

69. Jiang, J.; Oberdörster, G.; Elder, A.; Gelein, R.; Mercer, P.; Biswas, P. Does nanoparticle activity depend upon size and crystal phase? *Nanotoxicology* **2008**, *2*, 33–42. [CrossRef]

70. Kim, J.-P.; Lee, I.-K.; Yun, B.-S.; Chung, S.-H.; Shim, G.-S.; Koshino, H.; Yoo, I.-D. Ellagic acid rhamnosides from the stem bark of *Eucalyptus globulus*. *Phytochemistry* **2001**, *57*, 587–591. [CrossRef]

71. Santos, S.A.; Carmen, S.F.; Rosário, M.; Domingues, M.; Armando, J.D.; Carlos, P.N. Characterization of phenolic components in polar extracts of *Eucalyptus globulus* Labill. Bark by high performance liquid chromatography–mass spectrometry. *J. Agric. Food Chem.* **2011**, *59*, 9386–9393. [CrossRef]